American Journal of Polymer Science & Engineering
http://www.ivyunion.org/index.php/ajpse/

Research Article

Synthesis, Characterization and Properties of In-Situ Generated Polyimide/Silica/Polyoxometalate Hybrids via Sol-Gel Method

Ayesha Kausar[1,*] and Muhammad Siddiq[2]

[1]Nanosciences and Catalysis Division, National Centre For Physics, Quaid-i-Azam University Campus, Islamabad, Pakistan.

[2]Department of Chemistry, Quaid-i-Azam University, Islamabad, Pakistan

Abstract

In this research attempt, polyimide (PI) was prepared using 4-bromobenzene-1,3-diamine dihydrochloride and trimellitic anhydride chloride. The organic-inorganic nanocomposites were developed by means of TEOS and various content of polyoxometalate (POM). The silica network was synthesized in the polyimide matrix through *in-situ* sol-gel technique. FTIR was used to study the formation of polyimide and sol-gel nanocomposites. The physical properties of the *in-situ* prepared polyimide/silica/polyoxometalate nanocomposites were compared with those of neat polymer and polyimide/silica composite. Morphology study confirmed the homogeneous dispersion of silica phase in PI bulk phase with the formation of porous network structure. The glass transition temperature of the nanocomposites was in the range of 240-275 ℃, i.e. higher than the neat matrix (156 ℃). The melting peaks were also increased compared with the neat polyimide. Water uptake studies exhibited significant improvement in property for hybrids with higher POM content. In summary, PI/TEOS/POM 50 nanocomposite depicted improved thermal and water absorption properties along with the well-dispersed morphology.

Keywords: Polyimide; polyoxometalate; *in-situ*; sol-gel; glass transition; water uptake

Academic Editor: Taihong Shi, PhD, Sun Yat-sen University, China

Received: August 5, 2015; **Accepted**: September 29, 2015; **Published**: October 8, 2015

Competing Interests: The authors have declared that no competing interests exist.

***Correspondence to:** Ayesha Kausar, Nanosciences and Catalysis Division, National Centre For Physics, Quaid-i-Azam University Campus, 44000, Islamabad, Pakistan; **E-mail**: asheesgreat@yahoo.com

1. Introduction

Polyimides are an interesting category of extremely strong and remarkably chemical and heat resilient polymers. However, in several circumstances, they are not soluble and do not react at temperature lower than their decomposition temperature, which limits their requisitions as manufacturing materials [1]. Countless efforts have been performed to increase their ability of being processed while retaining their excellent mechanical and thermal features [2, 3]. For instance, flexile alkyl side chain, lateral bulky substituents, non-coplanar biphenyl based moieties as well as flexile aryl or alkyl ether spacers have been utilized to improve the solubility and hence processability [4, 5]. Integration of flexible functionalities (like SO_2–, –O–, –$C(CF_3)_3$, —$(CH_2–)_2$ and large pendulous groups (for example adamantyle and t-butyl) have been seen effective in varying intermolecular interaction and crystallinity to improve solubility [6, 7]. Unfortunately, pendant aliphatic sections and non-coplanar assembly that increase the solubility also usually decrease the thermal features. Recently, few spiro associated diamine derived soluble thermoplastic polyimides have been used to control this problem [8]. Such polymers had T_g's in the range of 200 to 250 ℃ and have been observed stable up to 500 ℃. Howbeit, such polyimides were insoluble with the exception of those integrating diphenylsulfone tetracarboxylic anhydride (DSDA) and hexafluoroisopropyledene-2,2'-diphthalic anhydride (6FDA) [9]. Organic-inoganic hybrid nanocomposites obtained by sol-gel procedure with *in-situ* grown inorganic phase have been actively followed world wide [10, 11]. The shift of emphasis from the conventional technique of mechanically mixing reinforcing fillers with polymer matrix towards the sol-gel method is generally owed to the refined control over morphology and/or surface features of the developing inorganic filler phase in the polymeric matrix. This method desires control over different reaction parameters such as pH, temperature, and concentration. More significantly, the organic-inorganic hybrid composites have the domain sizes typically in the range of 1 to 100 nm compared with the conventional composites which have macro-level domain sizes in the range of micrometer to millimeter scale [12]. Therefore, the organic-inorganic hybrid composites are generally optically transparent, even if microphase separation exists. Sol-gel composite preparation commonly centers on the development of the inorganic filler phase by the hydrolysis-condensation of alkoxysilanes such as tetraethoxysilane (TEOS) in an organic polymer solution. The process of TEOS hydrolysis-condensation is well recognized [13]. Fig. 1 describes the generation of three-dimensional silica network as the consequence of hydrolysis and condensation reactions of TEOS. Thus far, several hybrids have been prepared by this method using poly(ethylene oxide) [14], poly(methyl methacrylate) [15], poly(vinyl acetate) [16], Nafion [17], poly(vinyl alcohol) [18] and numerous other polymers. Polyoxometalates (POMs) is a category of molecularly demarcated inorganic metal oxide groups that have acquired specific consideration due to their requisitions in countless technological fields for instance biology, medicine, materials, and catalysis owing to their electronic, structural, and chemical versatility [19]. In accordance, the growth of POMs-comprising functional nanomaterials and nanodevices has been progressively increasing [20]. Moreover their functional features have also been studied which offer an incentive to the combination of polyoxometalates chemistry and nanoscience. Based on the exceptional redox features and an increased protonic conductivity of polyoxometalates, both Dawson and Keggin-type hetero polyanions have been widely implemented as long-time stable and highly selective redox catalysts [21]. The novelty of this work lies in the fact that the silica nanophase has been grown in-situ within the polyimide matrix and

POMs probably for the first time. The present paper describes a comparison of spectroscopic, morphological, thermal, mechanical, and water absorption properties of silica composites with those of polyimide and an attempt has been made to explain the properties with the structure of the nanocomposites. It is worth mentioning that nanocomposites based on polyimides and inorganic metal oxide clusters has commercial potential [22, 23].

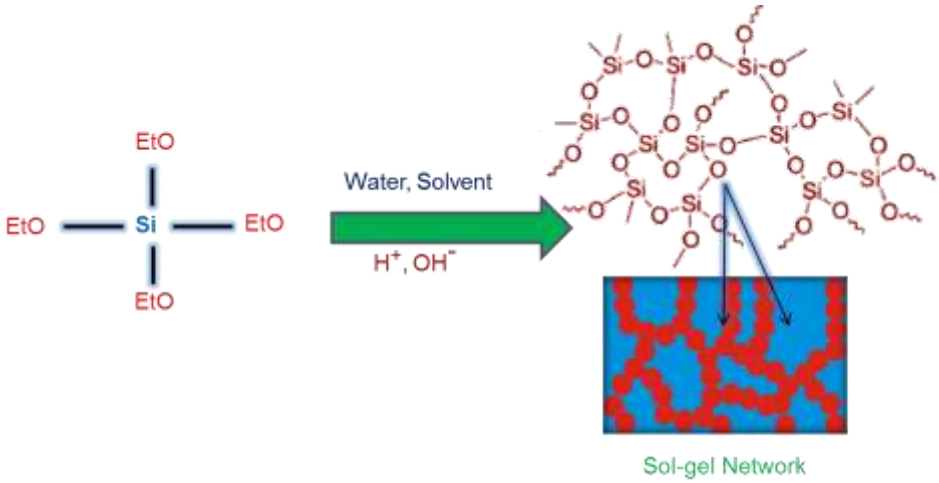

Fig. 1 Formation of 3D silica network during hydrolysis and condensation of TEOS.

2. Experimental

2.1. Materials

4-Bromobenzene-1,3-diamine dihydrochloride (BDD, 95 %), trimellitic anhydride chloride (TMAC, 99 %), tetraethyl orthosilicate (TEOS, 99.99 %, density 0.933) and dimethyl foramide (DMF, 98 %) were supplied by Aldrich. $H_3PMo_{12}O_{40}$ (POM) was purchased from Alfa Aesar.

2.2. Instrumentation

IR spectra were taken at room temperature with a resolution of 4 cm^{-1} using Excalibur Series FTIR Spectrometer, Model No. FTSW 300 MX manufactured by BIO-RAD. The scanning electron microscopic (SEM) images were obtained by Scanning Electron Microscope S-4700 (Japan Hitachi Co. Ltd.). The weight-average molecular weight (M_w) and polydispersity index (PDI) were calculated through gel-permeation chromatography (GPC). Differential scanning calorimetry (DSC) was performed by a METTLER TOLEDO DSC 822 differential scanning calorimeter taking 5 mg of the samples encapsulated in aluminum pans and heated at a rate of 10 °C/min under nitrogen atmosphere. Water absorption tendency of the nanocomposites was evaluated by immersing equal weights of the sample films in water for 120 h at ambient temperature. The water uptake was calculated using Eq 1.

$$\% \text{ Water uptake} = \frac{w_2 - w_1}{w_1} \quad (1)$$

Where,

w_1- Initial membrane weight (g)

w_2- Final membrane weight (g)

2.3. Preparation of polyimide

A 100 mL three necked round bottom flask containing 0.01 mol of BDD and 0.01 mol of TMAC and 25 mL of DMF were fitted with a magnetic stirring bar, condenser, nitrogen pad and a thermometer. The mixture was heated to 120 ℃ with stirring for 12 h. After heating this mixture for 8 h, it was cooled down to ambient temperature (Fig. 2). The mixture was poured into Petri dish and dried at 100 ℃ for 8 h to obtain film [3]. The M_w was found as 41×10^3 $gmol^{-1}$ and PDI was 2, according to GPC analysis.

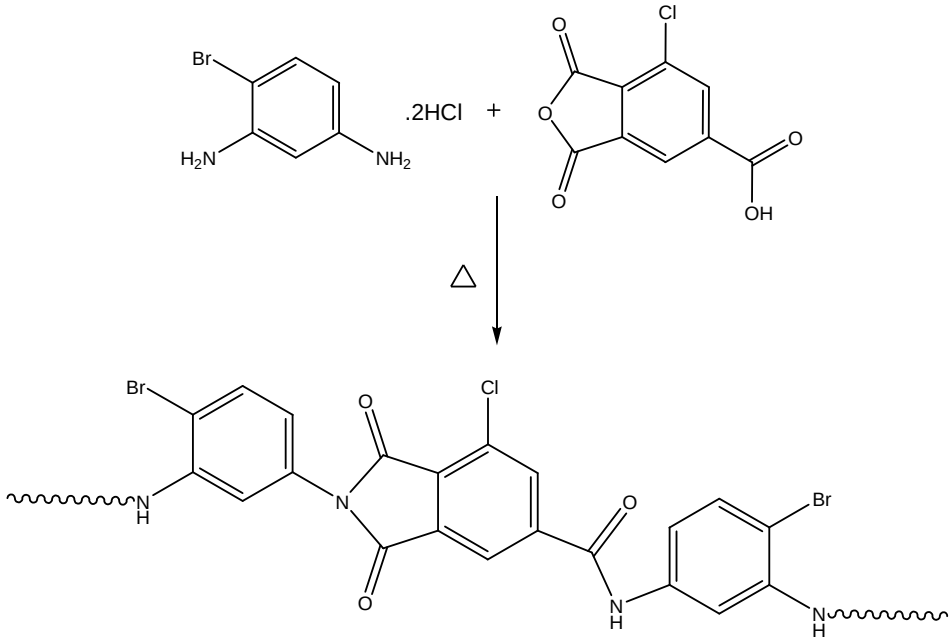

Fig. 2 Synthesis of polyimide

2.4. Preparation of polyimide/silica/POMs nanocomposite

0.01 mol of BDD and 0.01 mol of TMAC were dissolved in 25 mL of DMF. The mixture was heated to 120 ℃ with stirring for 12 h. 10 wt. % of TEOS was carefully added to this solution with vigorous stirring. Five drops of distilled water were added. The stirring was carried out for 1 h. Afterward the mixture was poured in 100 mL beaker and desired amount of POM (10-50 wt. %) was added under ambient conditions. The beaker was covered with polyethylene film and allowed to stand at room

temperature for 12 h to allow the hydrolysis and condensation reaction. Then finally mixture was poured in glass Petri dishes and dried at 100 ℃ for 10 h to obtain thin film. The films were stored in a desiccator to minimize moisture entrance [24].

3. Results and Discussion

3.1. FTIR studies

The FTIR spectra of polyimide and PI/TEOS/POM 10 are shown in Fig. 3 with all the characteristic peaks labeled. Fig. 3A shows characteristics peaks for the formation of polyimide. The symmetric and asymmetric imide C=O stretching vibrations were found at 1780 and 1731 cm^{-1}, whereas amide C=O stretch was found at 1680 cm^{-1}. The secondary amine N–H stretching and bending vibrations were observed at 3378 and 1599 cm^{-1}. The aromatic C–H stretching vibrations were located at 3111 and 3021 cm^{-1}. The spectrum of PI/TEOS/POM 10 is given in Fig. 3B. The secondary amine N–H stretching and bending vibrations were located around 3321 and 1590 cm^{-1}. The aromatic C–H stretching vibrations were located at 3109 and 3011 cm^{-1}. The characteristics symmetric and asymmetric imide C=O stretching vibrations were found at 1778 and 1720 cm^{-1}, while amide C=O stretch was found at 1670 cm^{-1}. The imide C–N stretch emerged at 1320 cm^{-1}. The peaks at 1022 and 1081 cm^{-1} in the IR spectrum of the silicate nanocomposite were assigned to the asymmetric Si–O–Si stretching [24]. The vibration at 811 cm^{-1} was linked with symmetric Si–O–Si stretching, while peak at 460 cm^{-1} emerged due to Si–O–Si bending mode. The peak centered at 3401 cm^{-1} was owing to hydrogen-bonded silanol SiO–H stretching vibrations. Moreover peak observed at 930 cm^{-1} was assigned to Si–OH (silanol) stretching vibration.

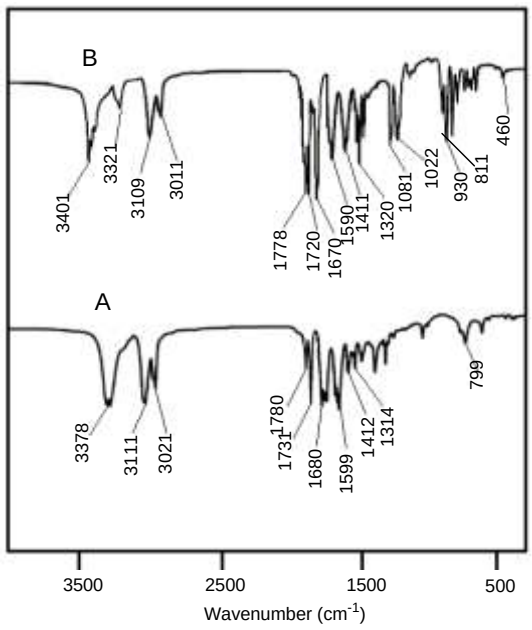

Fig. 3 FTIR spectra of (A) neat polyimide film and (B) PI/TEOS/POM 10 nanocomposite.

3.2. Microscopic studies

The FESEM phase images for PI/TEOS/POM nanocomposites are shown in Fig. 4. The morphology of PI/TEOS/POM 10 is shown in Fig. 4 A&B. The presence of fluffy porous structure was seemed to be predominant due to sol-gel network formation. The size of pores runs into the micron range while the width varies between 80-100 nm (Fig. 4B). Few discrete nano-sized silica particles were also dispersed throughout the matrix. Fig. 4C&D show the morphology of PI/TEOS/POM 50 nanocomposite. Some porous layered silica structure was found embedded in the polymer matrix. It was evident that the polymer/silica network became more distinguished with the higher POM loading (Fig. 4 D). Moreover, there was no aggregation in the nanocomposite films having POM loading of 50 wt. %. Since, there was no agglomeration of the silica particles in the nanocomposite film; therefore the transparency of the films was not much affected.

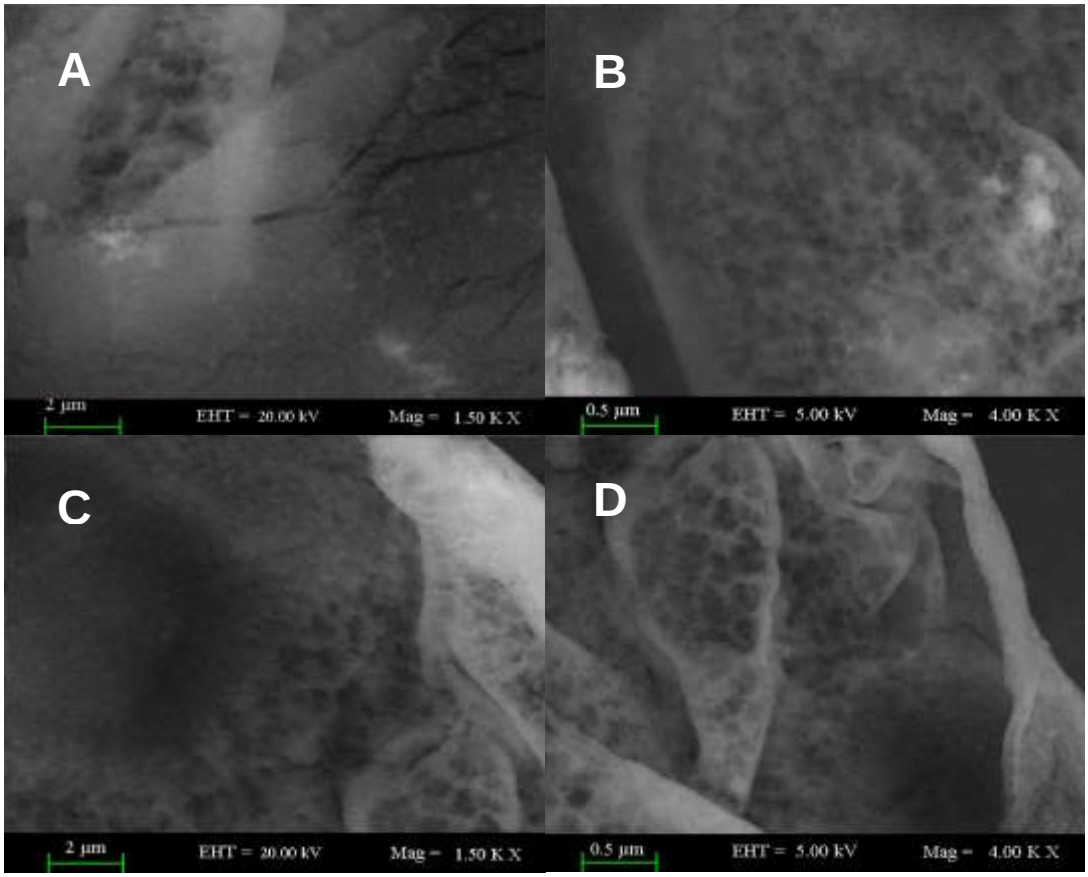

Fig. 4 FESEM images of (A) PI/TEOS/POM 10 (2 µm); (B) PI/TEOS/POM 10 (0.5 µm); (C) PI/TEOS/POM 50 (2 µm); and (D) PI/TEOS/POM 50 (0.5 µm).

3.3. Thermal characterization

The nanocomposite melting was studied by performing DSC on PI, PI/TEOS and PI/TEOS/POM 10-PI/TEOS/POM 50 series. The DSC traces of the samples are compared in Fig. 5. A summary of the DSC data corresponding to the curves for the heating scan are tabulated in Table 1. The data indicated that with increasing POM loading, the melting peaks were shifted towards right. The melting temperature was increased as well as the glass temperature (T_g) was enhanced. The obvious fact was that the *in-situ* generated sol-gel network caused increase in the crystallinity of nanocomposite. Thus, the incorporation of POM particles within the chain interstices increased the overall rigidity probably by enhancing the hydrogen bonding interaction between the inorganic oxides and N–H groups of polyimide backbone. The silanol groups are primarily responsible for this feature. According to the thermograms, the single melting phenomenon was ascribed to constant crystallite distribution in polyimide matrix. Furthermore, the appearance of melting peaks in all the nanocomposites indicated the nano-sized silica network generated in the system even at high POM loading. Analogous results have been reported in literature for polyimide/clay nanocomposites [25, 26]. In our nanocomposites, the glass transition temperature was increased with polyoxometalate loading; however various reported organoclay-based composites depicted lower thermal stability than the neat matrix [27].

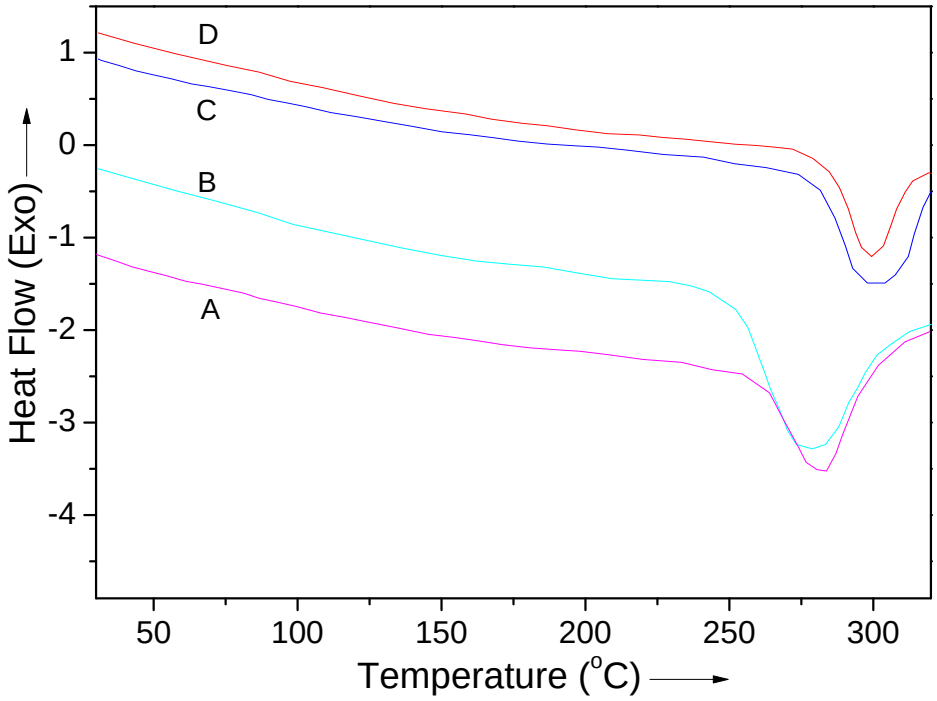

Fig. 5 DSC thermograms of PI/TEOS/POM films (A) PI/TEOS/POM 10; (B) PI/TEOS/POM 20; (C) PI/TEOS/POM 30; and PI/TEOS/POM 50 (D) at heating rate of 10 ℃/min in N_2.

Table 1 Glass transition temperature and % water uptake of nanocomposite films.

Composition	T_g (℃)	Water uptake (%)
PI	156	4.7
PI/TEOS	199	5.0
PI/TEOS/POM 10	240	5.2
PI/TEOS/POM 20	243	5.4
PI/TEOS/POM 30	254	5.7
PI/TEOS/POM 40	266	5.9
PI/TEOS/POM 50	275	6.2

3.4. Water absorption behavior

The water uptake characteristics of neat PI, PI/TEOS and PI/TEOS/POM 10-PI/TEOS/POM 50 series are presented in Table 1. Fig. 6 shows the comparative water uptake characteristics of PI/TEOS/POM 20 and PI/TEOS/POM 50 nanocomposites. The structure of pristine polyimide seems to be hydrophilic and tends to absorb water easily. From Fig. 6 it is seen that the PI/TEOS/POM 50 nanocomposite film has higher water absorbing tendency than PI/TEOS/POM 20. Similarly all the nanocomposites depicted higher water uptake compared with the polyimide and polyimide/silica films. The tendency can be explained on the basis of network formation. The TEOS sol-gel network structure formation led to increase in free volume of the polymer and formation of porous structure. The more porous structure of PI/TEOS/POM 50 nanocomposite aided the greater water absorption compared with that of PI/TEOS/POM 10. With increase in POM loading, the free volume of the polymer was increased further due to better polymerization of silica. Therefore, the water uptake of the polymer was increased with the increment of polyoxometalate loading.

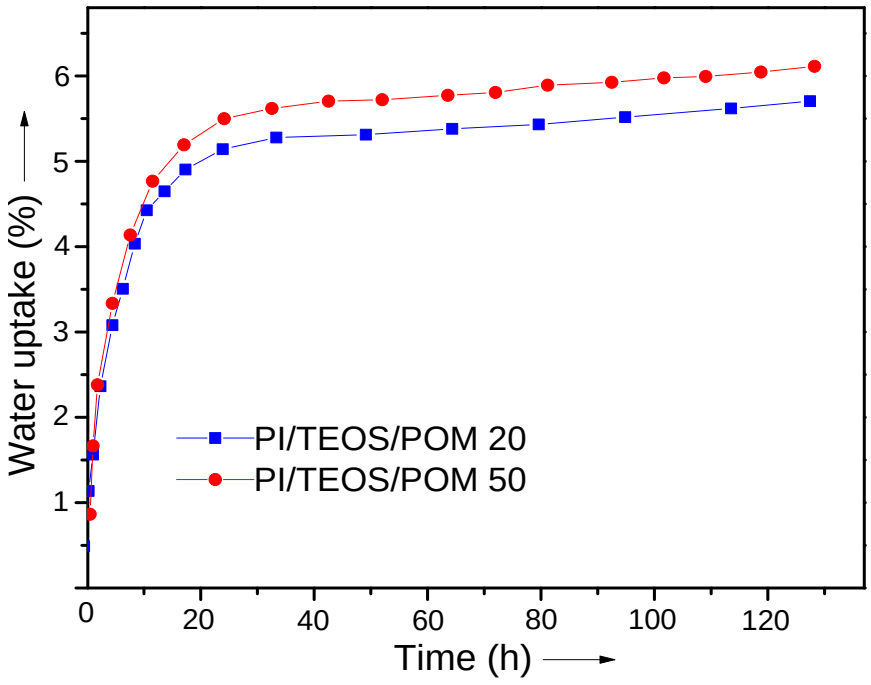

Fig. 6 Water uptake characteristics of PI/TEOS/POM nanocomposite.

4. Conclusions

The PI/silica/polyoxometalate hybrids were prepared by the sol-gel reaction between TEOS, POM and PI matrix. The properties of *in-situ* prepared polyimide/silica/polyoxometalate nanocomposites were compared with those of neat polymer and polyimide/silica composite. The synthesis of *in-situ* nano-silica network is a perspective method from the technological point of view. The structural studies revealed the formation of polyimide, polyoxometalate and *in-situ* grown silica network. SEM studies further confirmed that the silica structure was homogeneously dispersed in the bulk of the matrix. The DSC results indicated that the thermal stability enhancement was substantial even at very low loading of POM. Improvement in T_g of the hybrid films was observed relative to the neat film. Water absorption was continuously increased with POM loading due to increase in free volume of the polymer by the polymerized silica.

References

1. Jianga Q, Wang X, Zhu Y, Hui D, Qiu Y. Mechanical, electrical and thermal properties of aligned carbon nanotube/polyimide composites. ***Compos Part B: Eng***. 2014, 56:408-412

2. Kausar A, Hussain S T. Poly(azo-ether-imide) nanocomposite films reinforced with nanofibers electrospun from multi-walled carbon nanotube filled poly(azo-ether-imide). ***J Plast Film Sheet***. 2013, 30:266-283
3. Kausar A. A study on high performance poly(azo-pyridine-benzophenone-imide) nanocomposites via self reinforcement of electrospun nanofibers. ***Iran Polym J***. 2013, 23:127-136
4. Kausar A, Siddiq M. Structure and Properties of Buckypapers based on Poly(methyl methacrylate-co-methacrylic acid)/Polyamide 6,6 and Carbon Nanotube Intercalated Montmorillonite. ***J Compos Mater.*** 2015, DOI: 10.1177/0021998315586079
5. Nasir A, Kausar A, Younus A. A Review on Preparation, Properties and Applications of Polymeric Nanoparticle-based Materials. ***Polym-Plast Technol Engineer.*** 2015, 54: 325-341
6. Lee K M, Wang D H, Koerner H, Vaia R A, Tan L-S, White T J. Enhancement of photogenerated mechanical force in azobenzene-functionalized polyimides. ***Angewandte Chemie***. 2012, 124:4193-4197
7. Maktouf L B, Ghorbel I, Afli A, Abid S, Gandini A. Polyimides based on furanic diamines and aromatic dianhydrides: synthesis, characterization and properties. ***Polym Bull***. 2011, 67:1111-1122
8. Hsiao S-H, Wang H-M, Chen W-J, Lee T-M, Leu C-M. Synthesis and properties of novel triptycene-based polyimides. ***J Polym Sci A Polym Chem***. 2011, 49:3109-3120
9. Dhara M J, Banerjee S. Fluorinated high-performance polymers: Poly(arylene ether)s and aromatic polyimides containing trifluoromethyl groups. ***Prog Polym Sci***. 2010, 35:1022-1077
10. Armelao L, Barreca D, Bottaro G, Gasparotto A, Tondello E, Ferroni M, Polizzi S. Au/TiO_2 Nanosystems: A Combined RF-Sputtering/Sol−Gel Approach. ***Chem Mater***. 2004, 16:3331-3338
11. Kim D S, Park H B, Rhim J W, Lee Y M. Preparation and characterization of crosslinked PVA/SiO_2 hybrid membranes containing sulfonic acid groups for direct methanol fuel cell applications. ***J Membr Sci***. 2004, 240:37-48
12. Pandey S, Mishra S B. Sol–gel derived organic–inorganic hybrid materials: synthesis, characterizations and applications. ***J Sol-Gel Sci Tech***. 2011, 59:73-94
13. Tang F, Li L, Chen D. Mesoporous Silica Nanoparticles: Synthesis, Biocompatibility and Drug Delivery. ***Adv Mater***. 2012, 24:1504-1534
14. Ravaine D, Seminel A, Charbouillot Y, Vincens MJ. A new family of organically modified silicates prepared from gels. ***J Non-Cryst Solids***. 1986, 82:210-219
15. Landry C J T, Coltrain B K, Wesson J A, Zumbulyadis N, Lippert J L. In-situ polymerization of tetraethoxysilane in polymers. ***Polymer***. 1992, 33:1496-1506
16. Fitzgerald J J, Landry C J T, Pochan J M. Dynamic studies of the molecular relaxations and interactions in microcomposites prepared by in-situ polymerization of silicon alkoxides. ***Macromolecules***. 1992, 25:3715-3722
17. Stefanithis I D, Mauritz K A. Microstructural evolution of a silicon oxide phase in a perfluorosulfonic acid ionomer by an in situ sol–gel reaction. 3. Thermal analysis studies. ***Macromolecules***. 1990, 23:2397-2402
18. Suzuki F, Onozato K, Kurokawa Y. A formation of compatible poly(vinyl alcohol)/alumina gel composite and its properties. ***J Appl Polym Sci***. 1990, 39:371-381

19. Proust A, Matt B, Villanneau R, Guillemot G, Gouzerh P, Izzet G. Functionalization and post-functionalization: a step towards polyoxometalate-based materials. ***Chem Soc Rev***. 2012, 41:7605-7622
20. Gao L, Wang E B, Kang Z H, Song Y L. Layer-by-Layer Assembly of Polyoxometalates into Microcapsules. ***J Phys Chem B***. 2005, 109:16587-16592
21. Sadakane M, Steckhan E. Electrochemical Properties of Polyoxometalates as Electrocatalysts. ***Chem Rev***. 1998, 98:219-238
22. Liu S Q, Mo ̈hwald H, Volkmer D, Kurth D G. Polyoxometalate-based electro- and photochromic dual-mode devices. ***Langmuir***. 2006, 22:1949-1951
23. Gao L, Wang E B, Kang Z H, Song Y L. Layer-by-layer assembly of polyoxometalates into microcapsules. ***J Phys Chem B***. 2005, 109:16587-16592
24. Cheng S, Shen D, Zhu X, Tian X, Zhou D, Fan L-J. Preparation of nonwoven polyimide/silica hybrid nanofiberous fabrics by combining electrospinning and controlled in situ sol–gel techniques. ***Eur Polym J***. 2009, 45:2767-2778
25. Huang T-C, Hsieh C-F, Yeh T-C, Lai C-L, Tsai M-H, Yeh J-M. Comparative studies on corrosion protection properties of polyimide-silica and polyimide-clay composite materials. ***J Appl Polym Sci***. 2011, 119:548-557
26. Zhang Q, Li D, Lai D, You Y, Ou B. Preparation, microstructure, mechanical, and thermal properties of in situ polymerized polyimide/organically modified sericite mica composites. ***Polym Compos***. 2015, DOI: 10.1002/pc.23402
27. Kausar A. Bucky Papers of Poly(methyl methacrylate-co-methacrylic acid)/Polyamide 6 and Graphene Oxide-Montmorillonite. ***J Dispers Sci Technol.*** 2016, 37: 66-72